Journal of the European Ceramic Society 23 (2003) 273–282

www.elsevier.com/locate/jeurceramsoc

Structural studies of a ZrO_2–CeO_2 doped system

Valmor R. Mastelaro[a,*], Valérie Briois[b], Dulcina P.F. de Souza[c], Carlos L. Silva[c]

[a]*Instituto de Física de São Carlos, USP, C.P. 369 São Carlos, S.P., Brazil*
[b]*LURE-UPS, BP 34, Bât 209D, 91898 Orsay Cedex, France*
[c]*Departamento de Engenharia de Materiais, UFSCar, C.P. 679 São Carlos, S.P., Brazil*

Received 28 November 2001; received in revised form 6 May 2002; accepted 25 May 2002

Abstract

The local structure around Zr, Ce and dopant atoms (Fe and Ni) in the ZrO_2–CeO_2 system investigated by X-ray absorption spectroscopy (XAS) is reported to better understand the tetragonal phase stabilization process of zirconia. The first coordination shell around Zr atoms is not sensitive to the introduction of dopants or to an increase in the ceria content (from 12 to 20 mol%). Ce ions maintain the eight-fold coordination as in CeO_2, but with an altered bond distance. The formation of vacancies resulting from reduction of Ce atoms can be discarded, because XANES spectra clearly show that Ce ions are preferentially in a tetravalent state. XANES and EXAFS experiments at the Fe K-edge evidence that the local order around Fe is quite different from that of the Fe_2O_3 oxide. On the one hand, ab initio EXAFS calculations show that iron atoms form a solid solution with tetragonal ZrO_2. The EXAFS simulation of the first coordination shell around iron evidences that the substitution of zirconium atoms by iron ones generates oxygen vacancies into the tetragonal network. This is a driven force for the tetragonal phase stabilization process. For Ni doped samples, EXAFS results show that Ni–O mean bond length is similar to the distance found in the oxide material, i.e., NiO compound. Besides this result, no evidence of similar solid solution formation for Ni-doped systems has emerged from the EXAFS analysis

Keywords: EXAFS; Local structure; XANES; X-ray methods; ZrO_2–CeO_2

1. Introduction

Ceria stabilized tetragonal zirconia has attracted the attention in recent years due not only to its good mechanical and electrical properties,[1,2] but also to the possible applications of these materials as catalysts[3] and protective coatings against dry and wet corrosion of metallic alloys.[4]

Zirconium oxide, known as zirconia, has three polymorphic phases: monoclinic ($T<1170$ °C), tetragonal ($1170<T<2370$ °C) and cubic ($T>2370$ °C). The tetragonal and cubic phases can be obtained at room temperature with the addition of stabilizing ions.[5] Tetragonal zirconia can be stabilized by the addition of a small quantity of dopant oxide such as 3 mol% of Y_2O_3 or 12 mol% of CeO_2.[6,7] According to the literature,[6,7] the stabilization process of the tetragonal phase in the yttria–zirconia system results from the presence of oxygen vacancies, whereas it occurs in the ceria–zirconia system owing to the fact that oversized tetravalent Ce^{4+} atoms dilate the cation network, leading to a decrease of strain energy, which favors tetragonal stabilization.

During the synthesis of zirconia–ceria materials prepared by a traditional high temperature solid state reaction route, we observed that the tetragonal phase could not be retained at room temperature without the introduction of sintering aids.[8] It was found that dopants such as iron and copper lowered the sintering temperature from 1600 down to 1450 °C, with a percentage of tetragonal phase retained at room temperature higher than 98% and also with an increase of the electrical conductivity.[8] Mashio et al. studied the influence of sintering aids in the tetragonal phase stabilization process of the ceria–zirconia system.[9] They found that CuO and MnO_2, in a proportion of 0.3 mol%, are excellent sintering aids producing almost theoretically dense tetragonal zirconia ceramics with a small grain microstructure.

* Corresponding author. Tel.: +55-16-273-9755; fax: +55-16-273-9824.
E-mail address: valmor@if.sc.usp.br (V.R. Mastelaro).

0955-2219/02/$ - see front matter
PII: S0955-2219(02)00188-7

Although the short-range order structure of Zr and Ce atoms in the ZrO_2–CeO_2 system has been quite well studied,[7] the same cannot be said about the iron, nickel-doped ZrO_2–CeO_2 system. To better understand the contribution of sintering aids in the tetragonal phase stabilization process in zirconia–ceria system prepared by a solid state route, we undertook a structural study using an X-ray absorption spectroscopy (XAS) technique on a ceria-zirconia system doped with 0.3 mol% of iron and nickel. The XAS technique enabled us to probe the local structure of all the atoms present in the sample, even in low concentrations.

2. Experimental procedure

2.1. Materials

Zirconium oxide (Tosoh TZ-0), cerium oxide (Aldrich), $Fe_2(SO_4)_3$ (Aldrich) and $Ni(NO_3)_2.6H_2O$ (Aldrich) were mixed, using zirconia balls and isopropyl alcohol, to produce powders with the following nominal compositions: 88.0 mol% ZrO_2–12 mol% CeO_2 (Zr12Ce), 87.7 mol% ZrO_2–12 mol% CeO_2–0.3 mol% $Fe_2(SO_4)_3$ (Zr12CeFe), 87.7 mol% ZrO_2–12 mol% CeO_2–0.3 mol% $Ni(NO_3)_2.6H_2O$ (Zr12CeNi) and 79.7 mol% ZrO_2–20 mol% CeO_2–0.3 mol% $Fe_2(SO_4)_3$ (Zr20CeFe). The composition was implicitly recorded on each sample's label. Powders were dried at 50 °C to eliminate volatile species. Ball milled in isopropyl alcohol with the addition of 1.0 wt.% of polyvinyl butyral (PVB-Monsanto) were dried at room temperature and deagglomerated through an 80-mesh nylon sieve. 13-mm diameter discs were isostatically pressed at 270 MPa and sintered at 1450 °C for 1 h in air. These discs were used for all the measurements presented in this work.

2.2. XAS data collection

EXAFS (extended X-ray absorption fine structure) measurements were carried out at room temperature on the EXAFS IV beam line at LURE (the French synchrotron radiation facility), using the DCI storage ring (1.85 GeV and an average beam current of 300 mA). The monochromator used was a Si (111) for experiments made at the Ce $L_{III,}$ Ni and Fe K edges; and Si (311) for experiments made at the Zr K edge. The discs obtained after sintering were not ground for EXAFS experiments to avoid any tetragonal to monoclinic phase transformation. The Zr K edge and Ce L_{III} edge measurements were taken in total electron yield mode.[10] At least five scans were recorded for each sample in the energy interval 17 900–18 900 eV for the Zr K edge and 5700–6100 eV for the Ce L_{III} edge, respectively, using steps of 2 eV for the Zr K and 1 eV for Ce L_{III} edges. The XANES (X-ray absorption near edge structure) spectra at Ce L_{III} edge were recorded for each sample between 5700 and 5800 eV using steps of 0.3 eV. The Fe and Ni K edge measurements were carried out in fluorescence mode due to their small concentration (0.3 mol%). Fluorescence spectra were collected using a Si(Li) solid-state detector under an 800 eV energy range with 10s acquisition time per 2 eV energy step. Only Fe XANES spectrum has been recorded with a better resolution of 0.3 eV step. Several acquisitions (around 12 spectra) were carried out on the same sample to improve the signal to noise ratio.

2.3. EXAFS and XANES data analysis

All the EXAFS spectra were treated according to the single scattering approximation,[11,12] in line with the procedure described in Ref. 13. The EXAFS analysis was carried out by microcomputer using a program set written by Michalowicz,[14] according to the recommended procedures described by the International Workshop on Standards and Criteria in XAFS.[15] After atomic absorption removal and normalization, the $k^3\chi(k)$ weighted EXAFS signal was Fourier transformed to R distance space in the 2.5–13.4 $Å^{-1}$ limits for Zr, 3.1–9.7 $Å^{-1}$ for Ce, 2.8–11.8 $Å^{-1}$ for Fe and 3.0–10.8 $Å^{-1}$ for Ni. In each case, the Kaiser apodization window with $\tau = 2.5$ was used. The energy threshold was selected arbitrarily at the inflexion point of the absorption edge. The contribution of various neighboring shells was extracted by a back Fourier transform in R space and then fitted using experimental or theoretical phase and amplitude functions, depending on the backscatterer atom.

To model the Zr–O pair, the phase shift for the Zr–O pair and the oxygen backscattering amplitude were extracted from $BaZrO_3$ compound setting $N = 6$, $R = 2.09$ Å and $\sigma = 0.09$ Å. A quantitative analysis of the Ce–O shell was made taking a CeO_2 compound as reference ($R_{Ce\text{-}O} = 2.34$ Å and $N_{Ce\text{-}O} = 8$). Since it was impossible to obtain experimental amplitude and phase functions for the second neighbors contribution at the Zr and Ce edges, we used theoretical amplitude and phase functions to perform the simulation of Zr–cation and Ce–Cation interactions calculated using the FEFF program (Version 7.0).[16] The simulation of Fe–O interactions was performed using theoretical amplitude and phase functions calculated from FEFF program[15] whereas those used to simulate the Ni–O interactions was extracted from $Ni(OH)_2$ compound ($N = 6$, $R = 2.03$ Å). In all the fits, the number of free N_{par} parameters was kept smaller than the number of independent N_{ind} points, defined as $N_{ind} = 2\Delta R\Delta k/\pi$, where ΔR is the width of the R-space filter windows and Δk is the actual interval of the fit in the k space.[14]

For the fit made at the Zr and Ce edges, the errors were determined from the average standard deviation $\varepsilon(k)$ for a set of EXAFS spectra recorded for the same

sample. They are approximately equal to ±0.01 Å in distance and ±5% in coordination numbers for the first shell and equal to ±0.02 Å in distance and ±10% in coordination numbers for the second shell. The reliability of the fit was determined by the agreement factor ρ given in Ref. 17.

Ab initio EXAFS spectra characterizing iron dopant in substitutional site of tetragonal ZrO_2 network were calculated using the FEFF7 code in the single scattering framework. These simulations were based on the published structure of tetragonal ZrO_2[29] including a modification of Fe–O near neighbors distances supported by the EXAFS simulations performed on the first coordination shell.

A qualitative interpretation of XANES spectra obtained at the Ce L_{III} edge was performed using the software package developed by Michalowicz and Noinville.[18] For comparison purpose between different samples, all the spectra were background removed and normalized using as unity the inflexion point of the first EXAFS oscillation.

3. Results

Table 1 summarizes apparent density values and the percentage of tetragonal phase, grain size and sintering temperature for each sample.[8] The mechanical fragility of the Zr12Ce sample precluded measurements of its apparent density and grain size values. According to previous work,[8] the undoped sample (Zr12Ce) heat treated at 1450 °C displays the smallest percentage of tetragonal phase (around 18%), a 99.4 percentage of tetragonal phase could only be attained when the sample was heat-treated at 1600 °C. Comparing the doped samples, one can observe that for the samples heat-treated at 1450 °C the percentage of tetragonal phase is around 95.0–97.0% in the iron-doped samples and around 90.0% in the nickel one. The difference in the sintering temperature of 150 °C justifies then the use of dopants to obtain tetragonal zirconia. The average grain size for the Zr20CeFe and Zr12CeFe samples was found to be around 1.0 μm while, for the Zr12CeNi sample it was around 1.5 μm.

Table 1
Apparent density, percentage of the tetragonal phase and sintering temperature for samples characterized by EXAFS [28]

Sample	Apparent density (g/cm^3)	% Tetragonal phase	Average grain size (μm)	Sintering temperature (°C)
Zr12Ce	–	18.0	–	1450
Zr12CeFe	6.1	95.0	1.0	1450
Zr20CeFe	6.3	97.0	1.0	1450
Zr12CeNi	6.1	90.0	1.5	1450

3.1. EXAFS results: Zr K edge

The EXAFS signals and the corresponding Fourier Transforms (FT's) for undoped and doped samples are compared in Fig. 1a and b, respectively. The doped samples present similar EXAFS signal shapes, characteristic of the tetragonal phase. Although X-ray diffraction experiments detected the presence of 18% of tetragonal phase on the Zr12Ce sample, the EXAFS signal of this sample is characteristic of the monoclinic phase.[6]

The FTs (Fig. 1b) present two main peaks: one in the region between 1.1 and 2.3 Å, which is associated to the Zr–O bonding, while the region between 2.3 and 4.1 Å is mainly associated to the Zr–cation (cation = Zr,Ce) interactions. The peak located at approximately 6.7 Å in the doped samples, is known to be a fingerprint of the tetragonal phase.[6] It is attributed to multiple scattering processes that take place between a collinear array of scatters.[6]

The intensity of the first peak of the Fourier transform is similar in the three doped samples and faintly higher in the undoped sample. In regard to the second peak, only one peak is observed for the doped samples,

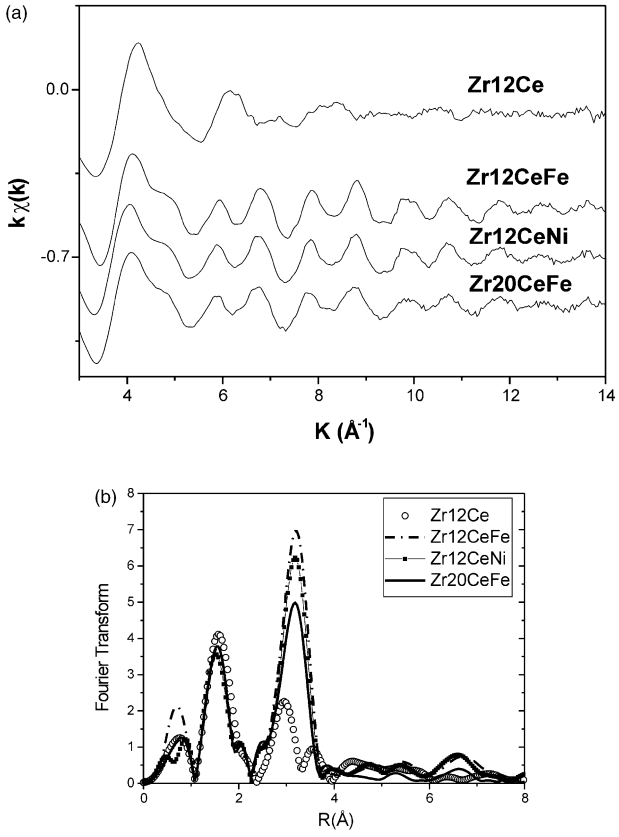

Fig. 1. (a) Experimental $k\chi(k)$ versus k EXAFS spectra and (b) amplitude of the Fourier transforms of $k^3\chi(k)$ for the samples Zr12CeFe, Zr12CeNi and Zr20CeFe. For the sake of clarity, each curve in Fig. 1(a) was shifted downward by a constant in relation to the preceding one.

whereas two resolved peaks with a reduced intensity are observed for the undoped sample. Moreover, in agreement with the reduction of intensity at high values of the EXAFS signal of the Zr20CeFe, a significant decrease of the intensity of the second peak for this sample can be observed.

Table 2 presents the fitting results for the first shell (Zr–O). In the first shell fitting procedure, interatomic distances (R), Debye–Waller factors (σ) and energy shift (ΔE) were allowed to vary, while the coordination numbers (N) were first fixed. Under these conditions, it was possible to obtain good fits. In agreement with the tetragonal structure (t-ZrO_2), which is composed of two subshells with 4 oxygen at short distance (2.10 Å) and 4 oxygen at long distance (2.35 Å), two subshells were used to fit the first shell of all doped samples. To test the validity of our simulations, we also allowed the coordination number to vary. Under these conditions, either the Debye–Waller factor or the coordination number changes appreciably (N varies from 3.9 to 4.1 for the doped samples). The undoped sample was also correctly adjusted considering a single shell procedure, in agreement with the monoclinic structure of this sample.[6]

The second peak of the Fourier transform (Fig. 1b), located between 2.3 and 4.1 Å, is mainly associated to Zr–cation (cation = Zr,Ce) interactions. The decrease of the intensity of the Zr–cation peak with the increase concentration of cerium has been correlated to an increasing static disorder.[7] However, Vlaic et al.[19,20] recently showed that decrease of the peak intensity results also from Zr–Zr and Zr–Ce phase functions out of phase, leading to destructive interference's between Zr–Zr and Zr–Ce pairs.

According to the literature,[5] the second shell around Zr atoms in the m-ZrO_2 phase is characterized by a broad distribution of Zr–Zr distances ranging from 3.34 to 4.54 Å. Due to the large number of fitting parameters involved in the monoclinic structure and the occurrence of a supplementary Zr–Ce contribution, we will not present the second shell simulation of the sample ZrCe12 that presents a monoclinic structure.

For the doped samples, we initially attempted to simulate the filtered second shell EXAFS spectra without the presence of Ce atoms, taking into account the existence of only 12 Zr atoms located at a medium distance of 3.62 Å and 24 O atoms located at a medium distance of 4.25 Å as reported for pure tetragonal zirconia.[6] The introduction of a Zr–O subshell at 4.25 Å improved the quality of the simulation, mainly at low k values. In a second trial, we introduced the contribution of Zr–Ce bonding, and the number of Zr–Zr and Zr–Ce contributions was calculated based on the sample's composition. For the Zr12CeFe and Zr12CeNi samples, the fitting quality in both cases (including or not the presence of cerium atoms in the second shell) are very similar, indicating that for these two samples we were not able to distinguish between both models. Consequently, the second shell analysis of these two samples was made assuming only the existence of Zr–Zr and Zr–O. On the other hand, we observed that the fitting quality of the Zr20CeFe sample is slightly improved when the contribution of cerium atoms is included in the fitting model. For this sample we included then the contribution of Zr–Ce atoms in the second shell fitting. The number of Zr–Zr and Zr–Ce contributions was in this case calculated based on the Zr20CeFe sample composition (the Zr–Zr coordination number was set to equal 9.3, mean bond length equal to 3.62 Å) and the Zr–Ce coordination number was set to equal 2.7 (mean bond length equal to 3.56 Å). Fig. 2 compares the filtered EXAFS experimental and theoretical curves for the Zr20CeFe sample without the presence of Zr–Ce atoms (and with the presence of Zr–Ce atoms). The second shell simulation results are also summarized in Table 2. Namely, X-ray diffraction results revealed the formation of a homogeneous solid solution between

Table 2
Results of the structural analysis of the first and second coordination shell at the Zr K edge[a]

Composition		Zr–O						Zr–Cation				
		N	R (Å)	σ (Å)	ΔE (eV)	ρ (%)		N	R (Å)	σ(Å)	ΔE (eV)	ρ (%)
Zr12Ce	Zr–O	7.0	2.14	0.10	8.7	0.7		–	–	–	–	–
Zr12CeFe	Zr–OI	4.0	2.10	0.08	4.4	0.4	Zr–Zr	12.0	3.62	0.09	−11.3	0.33
	Zr–OII	4.0	2.34	0.11	1.1		Zr–O	24.0	4.11	0.21	−11.8	
Zr12CeNi	Zr–OI	4.0	2.11	0.08	2.7	2.5	Zr–Zr	12.0	3.62	0.09	−13.7	0.25
	Zr–OII	4.0	2.35	0.10	−1.1		Zr–lO	24.0	4.11	0.23	−14.3	
Zr20CeFe	Zr–OI	4.0	2.11	0.08	3.6	4.2	Zr–Zr	9.3	3.61	0.09	−12.8	0.74
	Zr−OII	4.0	2.35	0.12	0.5		Zr–Ce	2.7	2.56	0.12	−12.8	
	Zr–O	24.0	4.25	0.22	−9.9		Zr–O	24.0	4.25	0.22	−9.9	

[a] N is the coordination number; R is the mean bond length with (±0.01 Å) for the first shell and with (±0.02 Å) for the second shell, σ (±0.01 Å) is the Debye–Waller factor and ρ is the agreement factor.

cerium and zirconia and this result is also supported by our EXAFS analysis.

3.2. XANES results: Ce L_{III} edge

Fig. 3 compares the Ce L_{III} XANES spectra of the zirconia–ceria samples with those of $CeRu_2Ge_x$ and CeO_2 references in which cerium atoms are trivalent and tetravalent, respectively. Two main peaks, *a* and *b*, separated by approximately 7 eV, can be observed in the CeO_2 spectra, in agreement with previous results.[21]

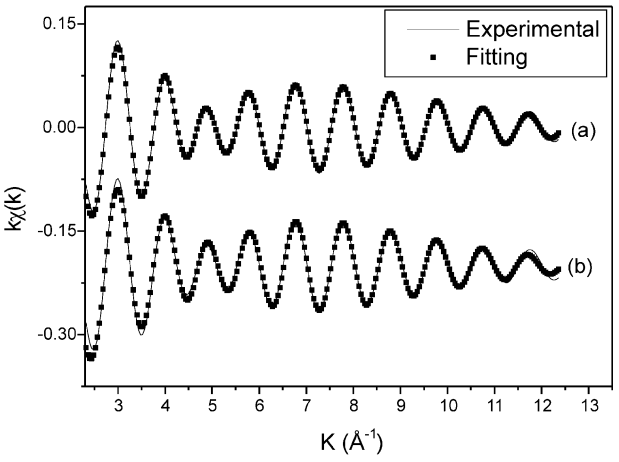

Fig. 2. Fit and back Fourier filtered signal of the second shell for the Zr20CeFe sample. (a) with the Zr–Ce contribution and (b) without the Zr–Ce contribution.

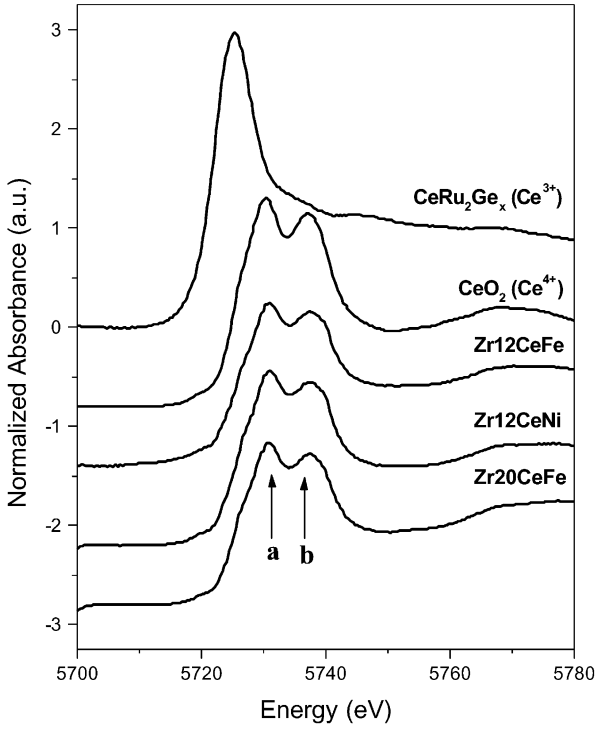

Fig. 3. XANES normalized absorption spectra at the Ce L_{III} edge.

These two components were also detected in the ceria–zirconia samples, with an intensity ratio close to that found in the CeO_2 sample. Although we can not completely excluded the presence of Ce^{3+} atoms in our samples, based on the comparison with the reference compounds, we can conclude that Ce atoms are preferentially in a tetravalent state. The energy difference between the *a* and *b* peaks in the XANES spectra of the zirconia–ceria samples is slightly smaller than in CeO_2: about 6.0 ± 0.2 eV for all the samples. This can be qualitatively explained by a shortening of the Ce–O distance. Although the Ce atom in zirconia–ceria samples is eightfold coordinated as in CeO_2, the Ce–O mean bond length is shorter. The shortening of distances of the first oxygen coordination shell for the zirconia–ceria samples compared to CeO_2 is also evidenced by the shift at higher energy of the first EXAFS oscillation according to the well known Natoli's rule.[22] In fact, the same behavior was observed by Ping Li et al.[7] in ZrO_2–CeO_2 samples and by Douillard et al. in Ce-doped Y_2O_3 samples.[21]

3.3. EXAFS results: Ce L_{III} edge

A comparison of the Fourier transforms of zirconia–ceria samples at the Ce L_{III} edge is given in Fig. 4. Concerning the first peak (Ce–O first coordination shell), the FT's of zirconia–ceria samples appear to present the same Ce–O distance. A large difference of the intensity of the second peak of the Fourier transforms is observed as a function of the ceria content.

Table 3 presents the first shell (Ce–O) fitting results. In the fitting procedure, the Ce–O first shell coordination number was allowed to vary during the simulation procedure. The spectra were reasonably simulated using a single-shell model. As expected, from the formation of a solid solution between Ce and ZrO_2, a coordination number close to 8 was obtained. The Ce–O mean bond length presents a mean value equal to 2.26 Å, shorter

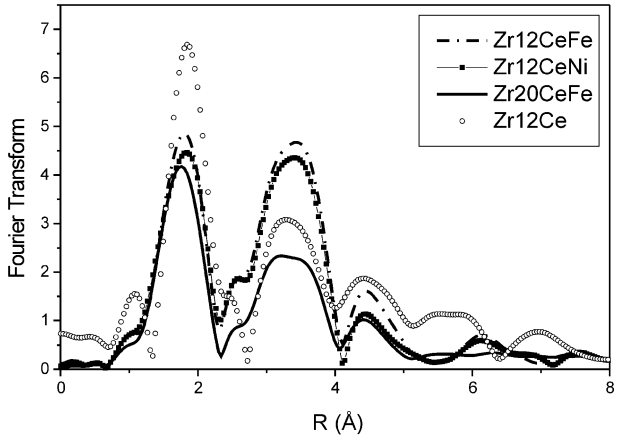

Fig. 4. Fourier transform at the Ce L_{III} edge for zirconia–ceria samples.

Table 3
Results of the structural analysis of the first and second coordination shell at the Ce L_{III} edge[a]

Composition	Ce–O						Ce–cation				
	N	R(Å)	σ(Å)	Δ*E* (eV)	ρ (%)		*N*	*R*(Å)	σ(Å)	Δ*E* (eV)	ρ (%)
CeO_2	8.0	2.34	–	–	–	Ce–Ce	12.0	3.82	0.04	4.5	7.6
						Ce–O	24.0	4.54	0.02	10.6	
Zr12Ce	8.1	2.27	0.08	−2.5	2.1						
Zr12CeFe	7.8	2.26	0.10	−1.7	1.5	Ce–Zr	10.0	3.57	0.00	−2.0	1.1
						Ce–Ce	1.9	3.87	0.00	−1.8	
						Ce–O	25.0	4.52	0.25	−3.7	
Zr12CeNi	7.8	2.26	0.11	−1.9	0.3	Ce–Zr	10.1	3.58	0.02	−1.4	1.4
						Ce–Ce	1.9	3.87	0.00	−3.4	
						Ce–O	24.0	4.54	0.25	−3.2	
Zr20CeFe	7.9	2.25	0.11	−2.0	1.6	Ce–Zr	9.5	3.56	0.06	−2.3	7.3
						Ce–Ce	2.5	3.85	0.09	−4.2	
						Ce–O	26.0	4.63	0.25	−1.1	

[a] *N* is the coordination number; *R* is the mean bond length with (±0.02 Å) for the first shell and with (±0.03 Å, ±0.04 Å) for the second shell [Ce–(Zr,Ce) and Ce–O respectively], σ (±0.01 Å) is the Debye–Waller factor and ρ is the agreement factor.

than the 2.34 Å observed in the CeO_2 sample, as previously deduced from the XANES results. The decrease in the Fourier transform first peak intensity for zirconia-ceria doped samples is explained by an increase of the Debye–Waller factor. The Ce–O mean bond length is relatively close to the Zr–O mean bond length in the tetragonal phase (2.22±0.02 Å).

As regards the second shell analysis, the consistency of the fitting results at the Zr K-edge should be checked with those obtained at the Ce L_{III} edge. As at the Zr K edge fitting, in an initial attempt, we assumed that the second shell around Ce atoms is formed only by Zr and O atoms. In the second attempt, we assumed that Zr, Ce and O atoms form the second coordination shell around Ce atoms. Contrary to what we observed at the Zr K edge, the simulation at the Ce L_{III} edge (second shell) was improved for all samples when the presence of Ce–Ce contribution in the second shell model were included. Fig. 5 compares the experimental and theoretical filtered EXAFS curves for the Zr20CeFe sample with the presence of Ce–Ce contribution and without the presence of Ce–Ce contribution. Table 3 summarizes the simulation results.

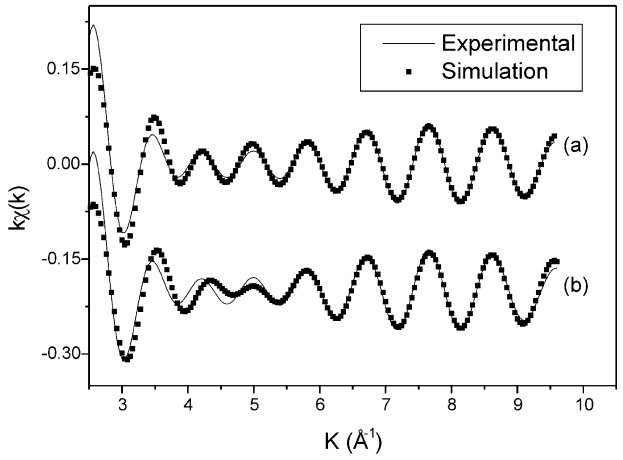

Fig. 5. Fit and back Fourier filtered signal of the second shell for the Zr20CeFe sample: (a) with the Ce–Ce contribution and (b) without the Ce–Ce contribution.

It is important to note that the same behavior is observed dealing with the disorder in the tetragonal structure, i.e., for a given 3d metal (Fe for example), when more Ce atoms are added, the structure becomes slightly more disordered. Furthermore, at a given Ce content, the addition of nickel ions systematically leads to a more disordered structure than does the addition of iron atoms.

3.4. EXAFS and XANES results: dopant K-edges

The interest of studying the local order around the dopants, Fe and Ni atoms, is due to the fact that, as was previously observed,[8] the introduction of these atoms in the ZrO_2–CeO_2 system decreases the sintering temperature and increases the percentage of tetragonal phase retained at room temperature. Thus, these atoms appear to be partially responsible for the improvement of the stabilization process in these zirconia–ceria samples.

Fig. 6 presents the Fe (sample Zr20CeFe) and Ni (sample Zr12CeNi) XANES spectra compared to the c-Fe_2O_3 (αphase) and c-NiO compounds, respectively. Despite of the poor resolution in the data acquisition, one can observe that the Ni K-edge XANES spectrum of Zr12CeNi sample is comparable to that of c-NiO oxide whereas the Fe Kedge XANES spectrum of

Zr20CeFe sample is quite different from the reference compound. In fact, the observed Fe XANES spectra of the Zr20CeFe sample is very similar to that obtained by Yamamoto et al. for the Fe sulfated zirconia samples[23] for which Fe atoms are proposed to be located at the center of a highly distorted octahedron.

The EXAFS raw spectra obtained at the Fe and Ni K-edges for the same samples are shown in Fig. 7. Fig. 8a compares the FT of Zr20CeFe to that of c-Fe_2O_3, while Fig. 8b is a comparison between the FT of the Zr12CeNi and the c-NiO samples. The presence of peaks at larger distances as displayed in the c-Fe_2O_3 and c-NiO oxide compounds, were not observed in zirconia–ceria doped samples. The structural parameters determined by a least square fitting procedure performed on the back Fourier transform of the first peak on the FT are gathered in Table 4. For the Zr20CeFe sample, a reasonable fitting was obtained when the EXAFS back Fourier transformed spectra was fitted with two shells ($N=3.9$ at 2.03 ± 0.02 Å and $N=2.7$ at 2.52 ± 0.02 Å), i.e., the total coordination number and the mean bond length were equal, respectively, to (6.6 ± 1) and $(2.27\pm0.02$ Å). The results obtained in this work for the first coordination shell of iron are totally in agreement with those reported by Yamamoto et al.,[23] in particular they confirm the distorted environment of iron. The refined iron-oxygen distances strongly suggest that iron substitutes zirconium in the tetragonal oxide network. Then we have

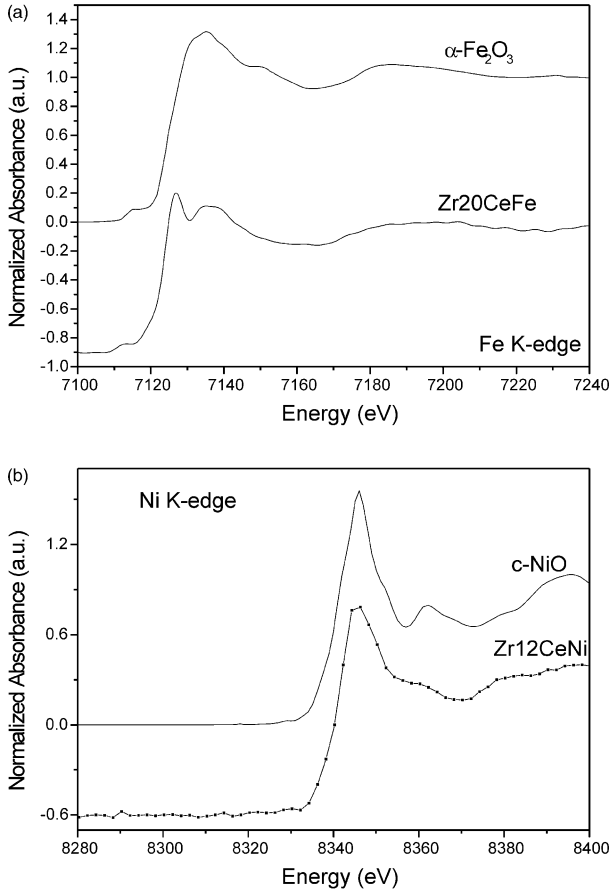

Fig. 6. XANES raw data at: (a) Fe K for the Zr20CeFe sample and (b) Ni K edge for the Zr12CeNi sample compared to the respective reference oxide samples.

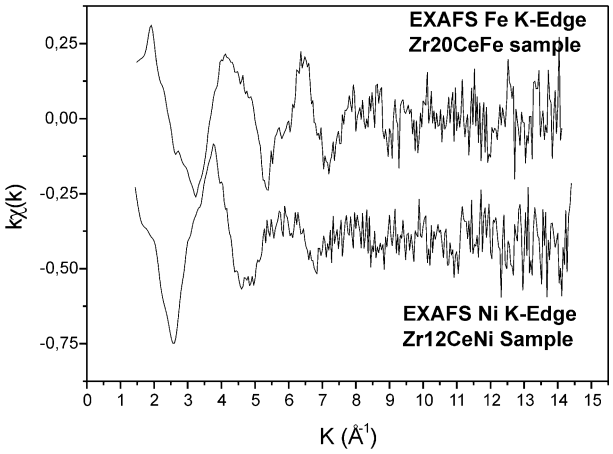

Fig. 7. Experimental $k\chi(k)$ versus k EXAFS spectra obtained at the Fe and Ni K edges for Zr20CeFe and Zr12CeNi samples.

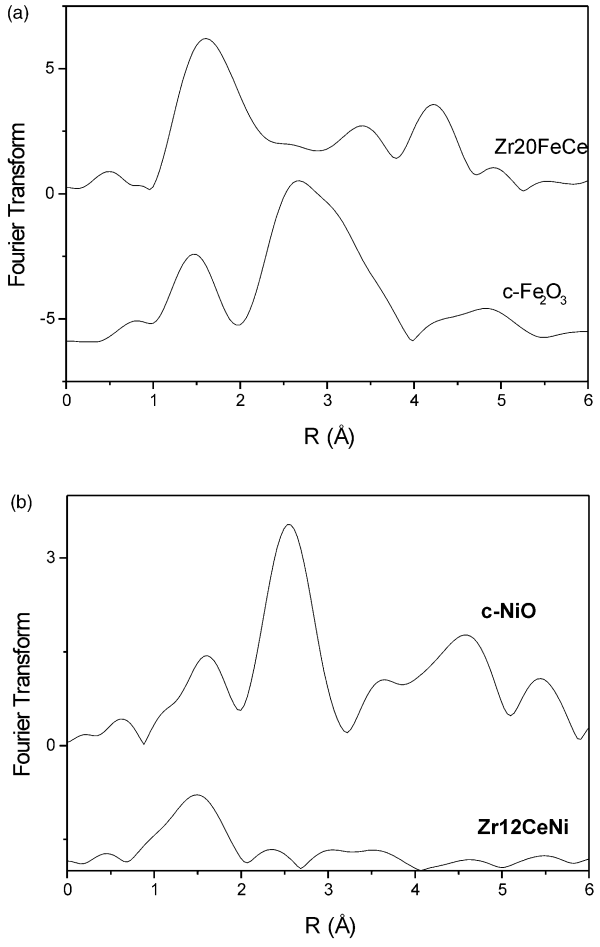

Fig. 8. Fourier transform obtained at the Fe (10a) and Ni (10b) K edges for Zr20CeFe and Zr12CeNi samples compared to the Fourier transform of oxide samples, Fe_2O_3 and NiO, respectively.

attempted ab initio EXAFS simulations for such substitution. Fig. 9 compares theoretical EXAFS spectrum to the experimental ones as well as the corresponding FT. The agreement between theory and experiment is satisfactorily and confirm that iron atoms in the Fe-doped ZrO_2–CeO_2 system form also a solution with ZrO_2. Similar conclusion was achieved for Fe-sulfated zirconia system reported in Ref. 23.

A Ni–O coordination number equal to (5.4±0.3) and a mean bond length approximately equal to (2.03±0.02 Å) were found for the Zr12CeNi sample. These parameters are very similar to that of NiO oxide compound.

4. Discussion

4.1. Local structure around zirconium, cerium, iron and nickel atoms

The analysis of the EXAFS results obtained at the Zr K-edge showed that the structure of the first shell (Zr–O_I and Zr–O_{II} bonding) is not sensitive to the introduction of dopants or to an increase in ceria content. The Zr first shell EXAFS simulations presented in this paper are in good agreement with those found in the literature.[7] However, contrary to that published by Ping Li et al.,[7] the simulations for the second shell around zirconium atoms show that the inclusion of Zr–Ce interactions in the second shell simulation improve the simulation results; principally for the Zr20CeFe sample. Thus for higher concentrations of cerium, the presence of Zr-Ce interactions must be taken into account.

In good agreement with previous works[7,21] we observed that Ce ions are maintained in a eightfold coordination, as in the CeO_2, in all the samples, albeit with a shortening of the bond distance. Thus, the "CeO_8" building block is more compressed in zirconia–ceria samples than in CeO_2. The consistency of the results obtained at the Zr K edge was confirmed by the results obtained at the Ce L_{III} edge in the second shell fitting. However, the fitting quality in this case was really improved for the three doped samples when we considered the presence of Ce–Zr and Ce–Ce interactions. Because the content of dopants was small, their contribution in the fitting was negligible. The XANES spectra analysis obtained at the Ce L_{III} edge clearly showed that the Ce ions are preferentially in the Ce^{4+} oxidation state.

The EXAFS analysis at the Ni K edge showed that the first Ni–O coordination number and the mean bond length are similar (considering the error bar) to that in the oxide sample, i.e., c-NiO. Then the possibility of oxide phase separation can not be ruled out for nickel doped ZrO_2–CeO_2 system. The EXAFS results at the Fe K edge clearly evidence the formation of a substitutional solid solution between iron and zirconium. These findings are in agreement with those published by Yamamoto et al.[23] and by Ping Li et al.[6]

Table 4
Results of the structural analysis of the first shell at the dopant K edges[a]

Composition	M–O				
	N	R(Å)	σ(Å)	ΔE (eV)	ρ
Zr20CeFe	3.9	2.03	0.08	4.4	0.9
	2.8	2.52	0.08	10.4	
Zr12CeNi	5.4	2.03	0.12	−2.8	0.06

[a] N is the coordination number; R is the mean bond length with (±0.02 Å) for the first, σ (±0.01 Å) is the Debye–Waller factor and ρ is the agreement factor.

4.2. Phase stability and tetragonality

It is well known that the stabilization process of a tetragonal phase at room temperature in the ZrO_2–

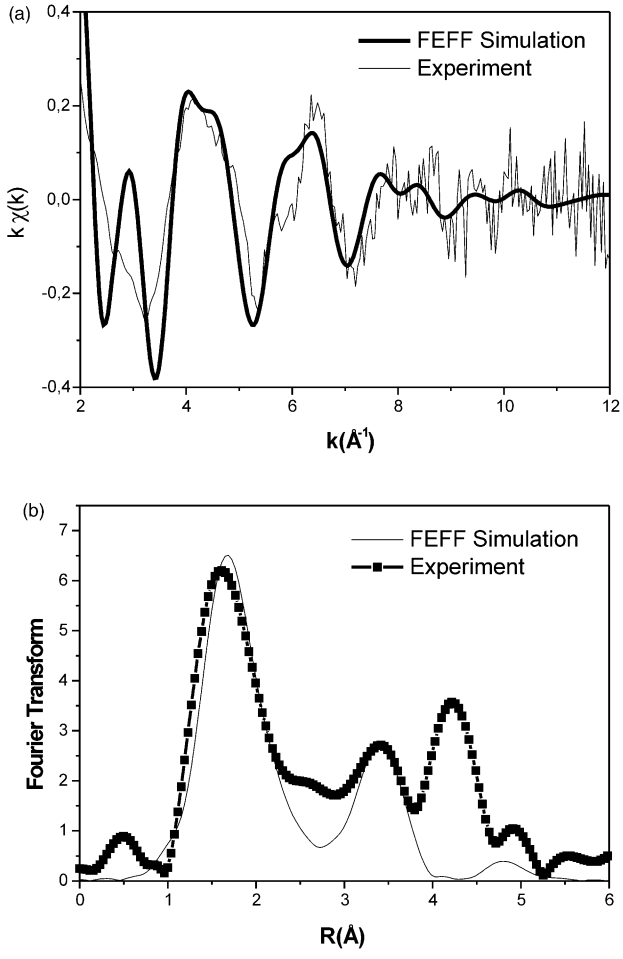

Fig. 9. Comparison between the experimental spectrum recorded at the Fe K edge for Zr20CeFe and the FeFF7 simulation obtained for iron atom in substitution of zirconium atom in the tetragonal network: (a) $k\chi(k)$ versus k EXAFS spectra and (b) corresponding Fourier transforms.

CeO_2 system may depend on several factors, such as grain size, dopant type and concentration and vacancy concentration caused by the introduction of dopants.[7–9,25–27]

As demonstrated earlier,[8] the Zr12Ce undoped sample presented only 18% of tetragonal phase, indicating that, in this case, the introduction of only 12% of CeO_2 to the zirconia lattice was not completely efficient to promote the total stabilization of the tetragonal phase. In the same sintering conditions (1450 °C), a large fraction of the tetragonal phase could be only retained at room temperature after doping the Zr12Ce sample with 0.3 mol% $Fe_2(SO_4)_3$ and $Ni(NO_3)_2.6H_2O$ compounds. Based on this information, some parameters are analyzed that may influence the stabilization process of the tetragonal phase at room temperature.

The scanning electron microscope (SEM) analysis of the samples studied in this work showed a grain size ranging between 1 and 2 μm (Table 1). This means that the stabilization process was not achieved by grain nanocrystalline size effect.[25]

Another possibility is that, as the samples are in pellet form, the tetragonal phase is retained at room temperature due to a compression effect. To verify this possibility, we measured the percentage of tetragonal phase in the pellet sample and in the powder sample obtained by grinding the pellet. The X-ray diffraction patterns of both samples are identical, indicating that the process of tetragonal phase stabilization was not achieved by a compression effect.

In a previous work,[28] we observed by transmission electron microscopy (TEM) that the introduction of iron as a sintering aid causes the formation of a liquid phase located in the microstructure triple points and along the grain boundaries as a very thin layer. This liquid phase formation improves the sample homogeneity during the sintering process enhancing the diffusion paths. This effect can promote a more efficient tetragonal phase stabilization process.

Mashio et al.[9] proposed that the stabilization process in a ceria-zirconia system containing sintering aids (such as CuO and MnO_2) is more effective because dopants introduce lattice defects and enhance cation diffusion through oxygen vacancy formation. Furthermore, they believe that when Ce^{4+} is reduced to Ce^{3+}, oxygen vacancies are introduced to balance its lower oxidation state. Our structural results indicate that Ce ions are preferentially in the Ce^{4+} state in every sample studied. This finding allowed us to discard the possibility of vacancy formation resulting from cerium reduction. As for Mashio's first assumption, our XAS results at the Fe K-edge show the formation of a solid solution in which the dopant substitute Zr atoms in the ZrO_2 structure. Since the total coordination number for Fe is equal to 7.0, its introduction generates oxygen vacancy, which will act in the stabilization process, as proposed by Mashio.[9] Contrary to iron EXAFS results we have found a regular first coordination shell around nickel, then the formation of similar solid solution is highly unlikely for the Zr12CeNi sample. Although the formation of NiO domains is not clearly evidenced by our EXAFS analysis, it is noteworthy that the formation of nanocrystalline oxide phase is expected to be less efficient into the tetragonal phase stabilization process[24] than the formation of solid solution between dopant and ZrO_2 host structure. Then, the difference in the proportion of tetragonal phase obtained by iron and nickel doping reported in Table 1 could be resulted from the formation of NiO domain in Zr12CeNi.

5. Conclusions

Our analysis of EXAFS results from the Zr K-edge showed that the structure of the first shell ($Zr–O_I$ and $Zr–O_{II}$ bonding) is insensitive both to the introduction of dopants and to the increasing ceria content. With regard to the second shell around zirconium atoms, the inclusion of Zr–Ce interactions in the second shell simulation failed to improve the simulation results.

Ce ions maintained the same coordination as in CeO_2 in all the samples, but with a shorter bond distance. Thus, the CeO_8 first coordination shell is more compressed in zirconia-ceria samples as compared to the CeO_2 structure. The analysis of XANES spectra obtained at the Ce L_{III} edge clearly showed that Ce ions are preferentially in the Ce^{4+} oxidation state. Thus, the formation of vacancies due to Ce atom reduction can be discarded.

The XANES spectra of iron doped sample is quite different from c-Fe_2O_3 allowing to rule out the possibility of phase separation. Ab initio EXAFS simulations have clearly evidenced that Fe atoms form a solid solution with ZrO_2 introducing by this way oxygen vacancies in the oxide network. The enhancement of the path diffusion caused by the introduction of oxygen vacancies improves the tetragonal phase stabilization process.

Finally we found that the first Ni–O mean bond length is similar to the distance found in NiO and no evidence of similar solid solution formation for Ni-doped systems has emerged from the EXAFS analysis.

Acknowledgements

The authors thank the team who ran the DCI synchrotron ring. The financial support from FAPESP, the Brazilian Research Funding Institution, is also fully appreciated. We are indebted to Professor Gilberto Vlaic from Trieste for the EXAFS data of the $BaZrO_3$ sample, and Professors Elson longo and Edson Leite from IQ-UFSCar, Brazil, for the critical comments.

References

1. Lai-Feng, Li, Yi-Yi, Li, Sbaizero, O. and Meriani, S., ZrO_2–CeO_2 alloys as candidate structural materials for cryogenic application. *J. Am. Ceram. Soc*., 1997, **80**(4), 1005–1008.
2. Chiodelli, G., Flor, G. and Scagliotti, M., Electrical properties of the ZrO_2–CeO_2 system. *Solid States Ionics*, 1996, **91**, 109–121.
3. Ranga-Rao, G., Fornasiero, P., Di Monte, E., Kaspar, J., Vlaic, G., Balducci, G., Meriani, S., Gubitosa, G., Cremona, A. and Graziani, M., Reduction of NO over partially reduced metal-loaded ZrO_2–CeO_2 solid solutions. *J. of Catalysis*, 1996, **162**, 1–9.
4. Di Maggio, R., Rossi, S., Fedrizzi, L. and Scardi, P., ZrO_2–CeO_2 films as protective coating against dry and wet corrosion of metallic alloys. *Surf. Coatings Technol*., 1997, **89**, 292–298.
5. Howard, C. J., Hill, R. J. and Reichert, B. E., Structures of the ZrO_2 polymorphs at room temperature by high-resolution neutron powder diffraction. *Acta Cryst. B*, 1988, **44**, 116–120.
6. Li, Ping, Chen, I-Wei and Penner-Hahn, James E., X-ray absorption studies of zirconia polymorphs I: local characteristic structure. *Phys. Rev. B*, 1993, **48**(14), 10063–10073.
7. Li, Ping, Chen, I-Wei and Penner-Hahn, James E., Effect of dopants on zirconia stabilization-an X-ray absorption study: II, tetravalent dopants. *J. Am. Ceram. Soc*., 1994, **77**(5), 1281–1288.
8. Foschini, C. R., Souza, D. P. F., Paulin Filho, P. I. and Varela, J. A., *J. Eur. Ceram. Soc*., 2001, **21**, 1143–1150.
9. Maschio, S., Sbaizero, O., Meriani, S. and Bischoff, E., Sintering aids for ceria-zirconia alloys. *J. Mater. Sci*., 1992, **27**, 2734–2738.
10. Tourillon, G., Dartyge, E., Fontaine, A., Lemmonier, M. and Bartol, F., Electron yield X-ray absorption spectroscopy at atmospheric-pressure. *Phys. Lett. A*, 1987, **121**, 251–257.
11. Sayers, D. E., Stern, E. A. and Litle, F. W., New technique for investigating noncrystalline structures—Fourier analysis of extended X-ray absorption fine structure. *Phys. Rev. Lett*., 1971, **27**, 1204.
12. Teo, B. K., *EXAFS: Basic Principles and Data Analysis*. Springer Verlag, Berlin, 1986.
13. Mastelaro, V., Benazeth, S., Dexpert, H., Ibanez, A. and Ollitrault-Fichet, R., A structural approach of the Ag–As–Se chalcogenide glasses: the Ag2Se–AsSe line. *J. Non-Cryst. Solids*, 1992, **151**, 1–12.
14. Michalowicz, A. EXAFS pour le Mac. In *Logiciels pour la Chimie*, Société Française de Chimie, Paris, 1991, pp. 102–103.
15. Anon., Report on the International Workshops on Standards and Criteria in XAFS, In *X-Ray Absorption Fine Structure: Proceedings of the VI International Conference on X-Ray Absorption Fine Structures*, ed S. S. Hasnain. Ellis Horwood, New York, 1991.p. 752.
16. Mustre de Leon, J., Rehr, J., Zabinsky, S. I. and Albers, R. C., *Phys. Rev. B*, 1991, **44**, 4146.
17. Chiavacci, L. A., Pulcinelli, S. H., Santilli, S. V. and Briois, V., Structural and phenomenological characterization of the thermoreversible sol-gel transition of a zirconyl aqueous precursor modified by sulfuric acid. *Chem. Mater*., 1998, **10**(4), 986–993.
18. Michalowicz, A. and Noinville, V. In *Gallad 2.0 code*, LURE, Orsay, France, 1992.
19. Vlaic, G., Andreatta, D. and Colavita, P. E., Characterization of heteregeneous catalysts by EXAFS. *Catalysis Today*, 1998, **41**, 261–275.
20. Vlaic, G., Navarra, G., Regnard, J. R., Willians, C.E and Jérome, R., EXAFS study of halato-telechelic polymers and capped with group IVB metal carboxylates at room and low temperatures. *J. Phys. II Fr*, 1995, **5**, 665–675.
21. Douillard, L., Gautier, M., Thromat, N., Henriot, M., Guittet, M. J., Duraud, J. P. and Tourillon, G, Local electronic structure of Ce-doped Y_2O_3: An XPS and XAS study. *Phys. Rev. B*, 1993, **49**(23), 16171–16180.
22. Natoli, C. R., Near edge absorption structure in the framework of the multiple scattering model. Potential resonance or chemical barrier effects?. In *EXAFS and Near Edge Structure—Chemical Physics,* vol 27, ed. A. Bianconi, L. Incorcia and S. Stipcich. Springer-Verlag, 1983, pp. 43–56.
23. Yamamoto, T., Tanaka, T., Takenaka, S., Yoshida, S., Onari, T., Takahashi, Y., Kosaka, T., Hasagawa, S. and Kudo, M., XAFS study of Fe- and Mn-promoted sulfated zirconia. *Journal of Synchrotron Radiation, Part 3*, 1999, **6**, 425–427.
24. Li, Ping, Chen, I-Wei and Penner-Hahn, James E., Effect of dopants on zirconia stabilization-an X-ray absorption study: I, trivalent dopants. *J. Am. Ceram. Soc*., 1994, **77**(1), 118–128.
25. Garvie, R. C., Hannink, R. H. and Pascoe, R. T., Ceramic steel. *Nature*, 1975, **258**, 703–704.
26. Becher, P. F. and Swain, M. V., Grain size dependent processing condition on the microstructure and transformation behaviour in Al_2O_3–$ZrO_2(CeO_2)$ composites. *J. Am. Ceram. Soc*., 1992, **75**(3), 493.
27. Bechepeche, A. P., Treu Jr, O., Longo, E., Paiva-Santos, C. O. and Varela, J. A., Experimental and theoretical aspects of the stabilization of zirconia. *J. Mater. Sci*., 1999, **34**, 2751–2756.
28. Silva, C. L. and de Souza, D. P. F., *Acta Microscopica*, 1998, **7**, 177.
29. Teufer, G., *Acta Cryst*, 1962, **15**, 1187.